Applications with Intense OTR Images II: Microbunched Electron Beams*

A.H. Lumpkin, R.J. Dejus, and D.W. Rule†

Advanced Photon Source, Argonne National Laboratory
9700 South Cass Avenue, Argonne, Illinois 60439 USA

Abstract. In this second application for intense images we take advantage of the coherent enhancement of optical transition radiation (OTR) due to self-amplified spontaneous emission (SASE) free-electron laser (FEL)-induced microbunching of the beam. A much smaller number of total particles is involved, but the microbunched fraction (N_B) gives a N_B^2 enhancement. We report measurements on the z-dependent growth of the coherent OTR (COTR) and the effects of beam size and electron beam/photon beam coalignment in the COTR interferograms.

INTRODUCTION

Coherent optical transition radiation (COTR) imaging techniques used for measuring the microbunching induced in the self-amplified spontaneous emission (SASE) free-electron laser (FEL) process have been successful in the VUV-visible regime. Besides the fundamental link to the SASE mechanism [1], one of the significant advantages is the enhancement of the COTR strength by several orders of magnitude compared to the incoherent process. In this second application we take advantage of this enhancement. This means that the standard imaging camera techniques can be employed as long as there are enough neutral density filters in place to keep the cameras out of saturation. This is not the "modus operandi" for OTR experiments with sub-nC-charge beams generally, but it can be for microbunched beams with bunching fractions of a few percent. In the case of the Advanced Photon Source (APS) SASE FEL, we have operated at wavelengths from 540 to 150 nm and observed the COTR z-dependent evolution easily [2-4]. In addition, we have clearly demonstrated that COTR interferograms contain fundamental information about effective e-beam size and the critical e-beam/photon beam overlap that can be used online to optimize gain.

EXPERIMENTAL BACKGROUND

The Advanced Photon Source facility includes an S-band linear accelerator, particle accumulator ring (PAR), booster synchrotron, and the 7-GeV storage ring (SR). During non-topup operations of the storage ring, the injector linac is available to

* Work supported by U.S. Department of Energy, Office of Basic Energy Sciences, under Contract No. W-31-109-ENG-38.
† NSWC, Carderock Division, West Bethesda, Maryland 20817 USA.

support the SASE FEL operations. For the SR injector an rf thermionic gun is generally used [5], but for the FEL we use the photocathode (PC) rf gun to generate the lower emittance and brighter beams [6]. A chicane at the 150-MeV point in the linac is used to compress the beam from a few-ps bunch length to sub-0.5-ps bunch lengths. The concomitant increase in peak current to around 400 to 500 A while maintaining 4 to 6 π mm-mrad emittance with about 0.1% energy spread provides reasonable gain for FEL operations from 540 to 150 nm. A schematic of the facility is shown in Fig. 1, and the parameters are summarized in Table 1.

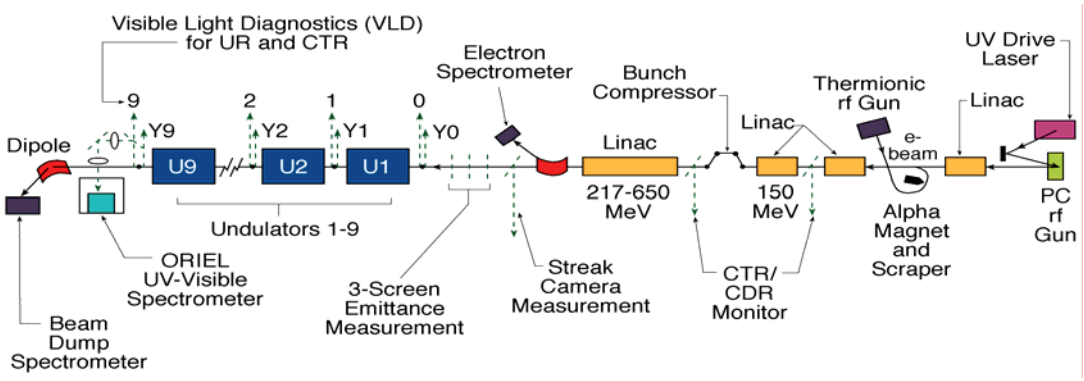

FIGURE 1. A schematic of the APS SASE FEL facility showing the PC rf gun, the linac, bunch compressor, matching stations, and the undulator area.

TABLE 1. Nominal Electron Beam Parameters with the PC-gun Beam Injected into the Undulators during the Experiments.

Parameter	Value
Beam Energy (MeV)	217, 308, 400
Emittance x,y (mm-mrad)	4-6
Peak Current (A)	300 to 500
Bunch Length (ps rms)	0.5
Charge (pC)	300-400
Energy Spread (%)	0.1-0.2

The undulator hall contains presently eight 2.4-m-long undulators with a period $\lambda_u = 3.3$ cm and K = 3.1. Before and after each undulator are optical diagnostic stations. We have previously reported and described the UV-visible systems, and we now have upgraded five of these stations with VUV-to-visible light imaging capabilities using reflective optics and in-vacuum CCD cameras [7]. A schematic of the upgrade stations located after undulators 2, 4, 5, 6, and 7 is shown in Fig. 2. The first translator provides for a YAG:Ce-mirror combination, an optical mirror at 45°, or a thin, 6-μm Al foil. The retractable mirror directs VUV-visible radiation to the VUV camera. The thin foil and this mirror have a separation of 63 mm to form the COTR interferometer.

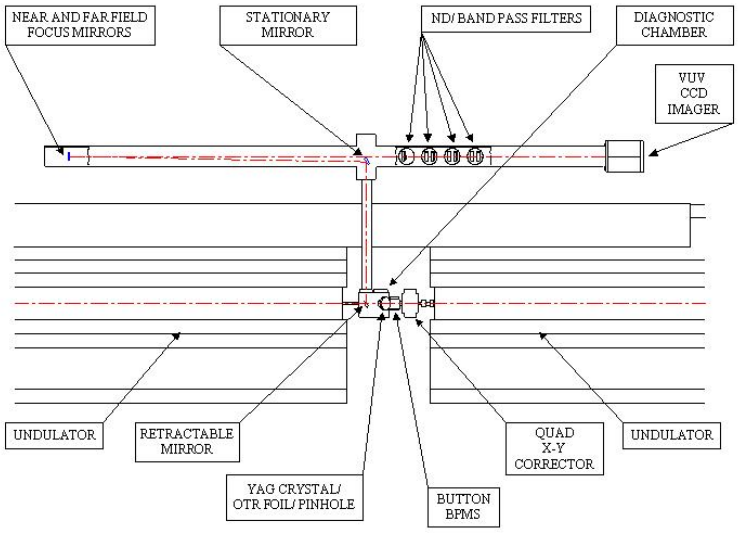

FIGURE 2. A schematic of the VUV-visible diagnostics station located after undulators 2, 4, 5, 6, and 7. Both SASE and COTR data in the near and far field can be taken with this system.

OPTICAL TRANSITION RADIATION BACKGROUND

Optical transition radiation (OTR) is generated when a charged-particle beam transits the interface of two media with different dielectric constants (e.g., vacuum to metal). The techniques have been more widely employed with electron beams, but so far only a few labs have looked at coherent OTR (COTR) and used COTR interferometry (COTRI). Overall, the techniques provide information on transverse position, transverse profile, divergence and beam trajectory angle, emittance, intensity, energy, and bunch length. There are coherence factors for wavelengths longer than the bunch length and for microbunched beams such as induced by a SASE FEL process [8].

It is this latter process that we have explored with the concomitant intense images. We use a model developed previously [8] to show the first direct comparisons of our COTRI data and calculations. The model describes the phenomenon in the spatial-angular distribution as a product of several functions as shown in Equation (1):

$$\frac{d^2N}{d\omega d\Omega} = \left|r_{\perp,\parallel}\right|^2 \frac{d^2N_1}{d\omega d\Omega} I\left(\boldsymbol{k}\right)\mathcal{F}\left(\boldsymbol{k}\right), \tag{1}$$

where the single particle OTR distribution is

$$\frac{d^2N_1}{d\omega d\Omega} = \frac{e^2}{\hbar c}\frac{1}{\pi^2\omega}\frac{\left(\theta_x^2+\theta_y^2\right)}{\left(\gamma^{-2}+\theta_x^2+\theta_y^2\right)^2}, \tag{2}$$

and where θ_x and θ_y are measured with respect to the angle of specular reflection, $\frac{e^2}{\hbar c} = \alpha$ is the fine structure constant, $I(\boldsymbol{k})$ is the interference term, and $\mathcal{F}(\boldsymbol{k})$ is the coherence function.

$I(\boldsymbol{k})$ is given by

$$I(\boldsymbol{k}) = 4\sin^2\left[\frac{kL}{4}\left(\gamma^{-2} + \theta_x^2 + \theta_y^2\right)\right], \tag{3}$$

where L = foil separation and $\boldsymbol{k}$ is the wave vector, and the coherence function

$$\mathcal{F}(\boldsymbol{k}) = N + N_B\left(N_B - 1\right)\left|H(\boldsymbol{k})\right|^2, \tag{4}$$

where the bunching fraction $f_B = N_B/N$, and $H(\boldsymbol{k})$ is the Fourier transform of the charge form factors.

The coherence function reduces to just the number of particles N when the number of microbunched particles N_B is zero. For the 540-nm case, we have f_B at 10 to 20% so the coherence enhancement of OTR is several orders of magnitude!

The 540-nm COTRI patterns have an unusual sensitivity to electron beam size compared to OTRI as shown in Fig. 3 for a 220-MeV beam energy and 0.2-mrad divergence. Here, the different beam form factors for the 100-, 50-, and 25-μm sizes and 0.2% bunching fraction explicitly enhance different peak fringes. The smallest beam size with largest form factor in θ-space enhances the first three fringes compared to only the inner lobes for the 50- and 100-μm sizes. The sensitivity is less in the 100-, 150-, 200-μm regimes as shown in Fig. 4, but there are still detectable differences. Basically the OTRI fringe peaks act as a built-in metric.

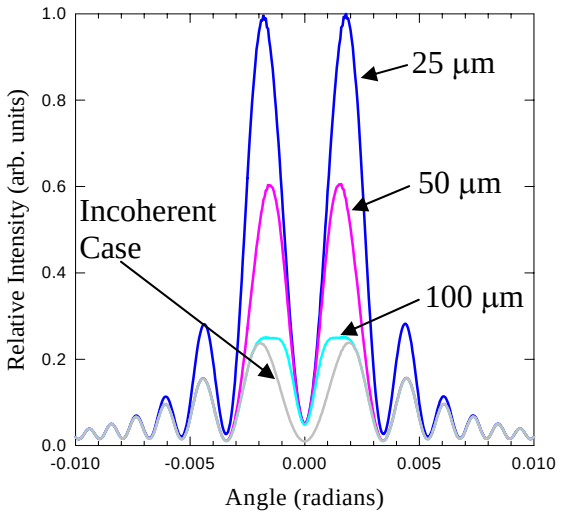

FIGURE 3: Calculations showing the effects of beam sizes of 100, 50, and 25 μm on the COTRI fringe peak relative intensities. The cofactor is larger in angular space for the 25-μm beam size and multiplies out to the third lobe's distribution in this case.

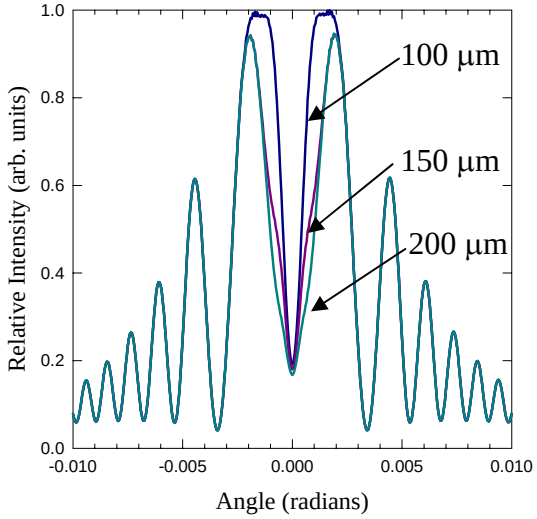

FIGURE 4: Calculations showing the effects of beam sizes of 200, 150, and 100 μm on the COTRI fringe peak relative intensities. The cofactors are narrow in angular space and only multiply the inner lobe distribution for this parameter set.

EXPERIMENTAL RESULTS AND COMPARISONS TO MODEL

Besides tracking the z-dependent growth of COTR in the exponential gain regime as shown in Fig. 5 where COTR increased by 10^4, we have found that the COTRI pattern image in the far field reveals effective beam size, and the symmetry of the pattern is related to beam coalignment in angle space. Our classic example of a beam image in the saturation regime (z = 19 m) of a SASE FEL was reported previously [2]. The model comparison to the data are shown here in Fig. 6 for θ_x and Fig. 7 for θ_y. The two inner lobes are seen with a fit of 75-μm effective size in Fig. 6 and the three fringe data of Fig. 7 are fit with a split-Gaussian beam size of 20 μm for negative angles and 25 μm for positive angles. The inner lobes are matched but the second

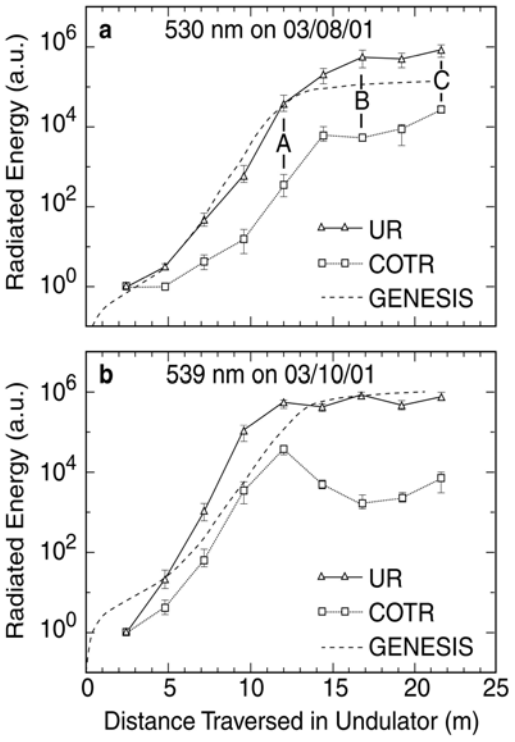

FIGURE 5. Plots of the *z*-dependent gain curves for the SASE undulator radiation (UR) and the COTR. The significant enhancement of COTR up to *z* = 12 m is clear (ref. 2).

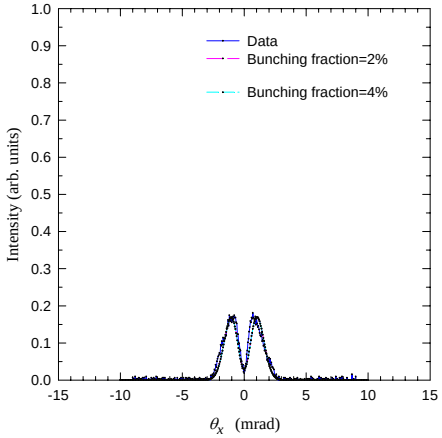

FIGURE 6. A direct comparison of model results and experimental θ_x data for the saturated regime case at 540 nm using a 75-μm beam size.

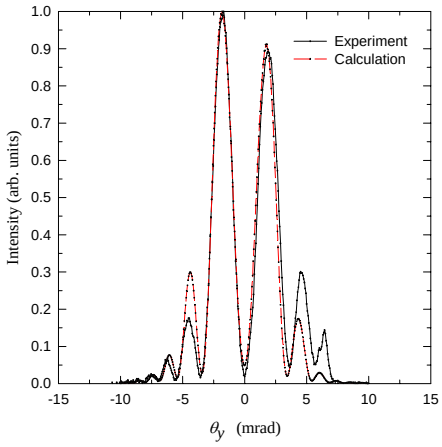

FIGURE 7. A direct comparison of model results and experimental θ_y data for the saturated regime case at 540 nm.

fringe peaks are not. The third and fourth are matched for negative angles with the 20-μm case. The effective beam sizes are smaller than the expected σ_x = 200 μm and σ_y = 100 μm based on the lattice and emittance. This aspect is consistent with microbunching having a transverse dependence.

An example of the electron-beam steering guided by the COTRI image symmetry is shown in Fig. 8. The top image at 540 nm is before the guided steering. This was the state after steering based on the intensity of the image after undulator 8. The normal fluctuations make it difficult to do fine tuning. However, by observing the image we used the corrector just before undulator 8 to steer the e beam until we obtained COTRI image symmetry in θ_x and θ_y. We then processed 100 images in each state and determined that both SASE and COTR gain had improved by a factor of 3 [9].

In the VUV regime at 157 nm, the beam energy is now 400 MeV so the natural opening angle is 1.2 mrad in OTR. But, the product with bunch form factors narrows the COTR lobes to the 0.5-mrad and 0.7-mrad levels for negative and positive θ_x, respectively, as shown in Fig. 9. It takes a split-Gaussian assumption since the symmetric 50-50-μm case will not work. The closest match is with the 43-25-μm set. The 25-μm beam cofactor works well for the first lobe and positive θ_x. The angular field of view of the camera is only ±2.5 mrad. The product function does not pick up the outer lobes. Issues of a bunch form factor center shift relative to the single electron function and the effects on peak intensity symmetry are being addressed.

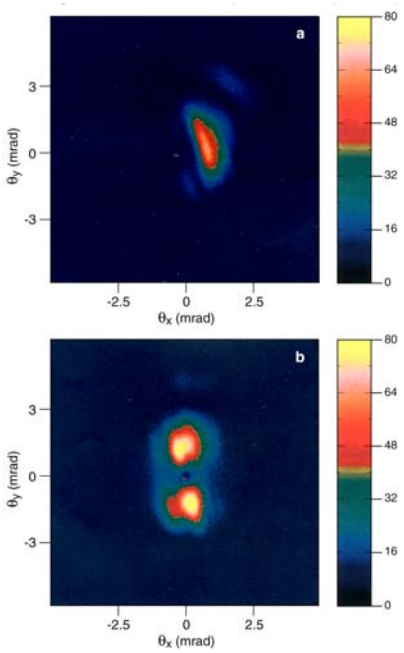

FIGURE 8. The COTRI images taken a) before and b) after the e-beam steering was done guided by image symmetry as observed after undulator 8 (ref. 9).

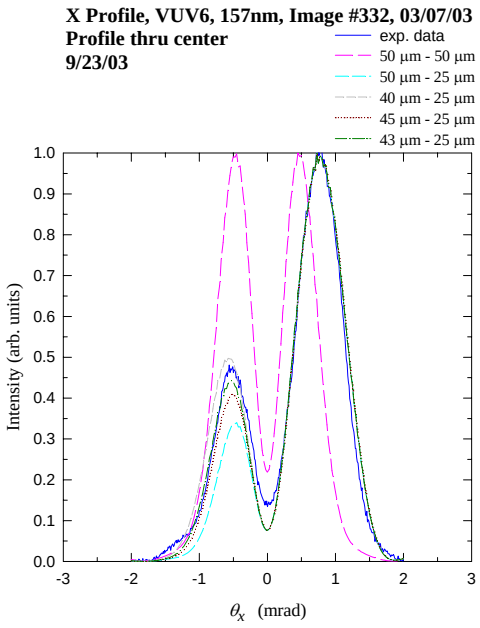

FIGURE 9. A direct comparison of model results and experimental θ_x data for VUV data at 157 nm. A split-Gaussian beam size and form factor are used to match the data.

SUMMARY

In summary, we have reported the distinct advantages of using COTR from microbunched beams due to the image intensity and structure dependence of the interferometric images on beam size and divergence. We have also described the sensitivity of COTRI to coalignment of the e-beam and SASE FEL photon beam as a gain optimization technique. The combination of these aspects provides a valuable complement to the diagnostics for SASE FELs.

ACKNOWLEDGEMENTS

The authors acknowledge the support of Kwang-Je Kim of the Accelerator Systems Division and members of the APS FEL team, particularly J.W. Lewellen and S.V. Milton, during the earlier experiments.

REFERENCES

1. Y.S. Derbenev, A.M. Kondratenko and E.L. Saldin, Nucl. Instrum. Methods, Vol. 193, 452 (1982).
2. A.H. Lumpkin et al., Phys. Rev. Lett., Vol. 86, 79 (2001).
3. A.H. Lumpkin et al., Phys. Rev. Lett., Vol. 88, 234801 (2002).
4. A.H. Lumpkin et al., "First Observations of COTR due to a Microbunched Beam in the VUV at 157 nm," Nucl. Instrum. Methods (in press 2004).
5. J.W. Lewellen et al., Proc. of the 1998 Linac Conference, Chicago, IL, ANL-98/28, Vol. 2, pp. 863-865 (1999).
6. S. Biedron et al., Proc. of the IEEE 1999 Particle Accelerator Conference, New York, NY, pp. 2024-2026 (1999).
7. P. Den Hartog et al., Nucl. Instrum. Methods, A483, 407 (2002).
8. D.W. Rule and A.H. Lumpkin, Proc. of the IEEE 2001 Particle Accelerator Conference, Chicago, IL, pp. 1288-1290 (2001).
9. A.H. Lumpkin et al., "On-line SASE FEL Gain Optimization using COTRI Imaging," Nucl. Instrum. Methods (in press 2004).